IEEE Access
Multidisciplinary | Rapid Review | Open Access Journal

Received May 4, 2020, accepted May 10, 2020, date of publication May 14, 2020, date of current version May 28, 2020.

Digital Object Identifier 10.1109/ACCESS.2020.2994614

Underwater Single Image Dehazing Using the Color Space Dimensionality Reduction Prior

YONGBIN LIU, SHENGHUI RONG, XUETING CAO, TENGYUE LI, AND BO HE, (Member, IEEE)

Underwater Vehicle Laboratory, School of Information Science and Engineering, Ocean University of China, Qingdao 266100, China

Corresponding authors: Shenghui Rong (rsh@ouc.edu.cn) and Bo He (bhe@ouc.edu.cn)

This work was supported in part by the project funded by the China Postdoctoral Science Foundation under Grant 2019M652472, and in part by the Fundamental Research Funds for the Central Universities under Grant 201813019 and Grant 201861009.

ABSTRACT Underwater images suffer from low visibility and contrast caused by absorption and scattering, which leads to haze and some further limitations. The existing underwater single image dehazing methods cannot achieve a balance between the performance and computational complexity, and are difficult to produce satisfactory results in the regions with large distance. To overcome these problems, we propose a new underwater single image dehazing method, which includes an improved background light estimation based on the quad-tree subdivision iteration algorithm, and a novel transmission estimation method. For the background light estimation, we introduce a robust score for each region of the image, which can evaluate the region from both smoothness and color. For the transmission estimation, we propose the color space dimensionality reduction prior (CSDRP), which allows conversing an image from the three-dimensional RGB color space to a 2D color space, namely the UV color space. In the UV color space, by clustering the pixels into mounts of haze-lines and carefully setting the haze-free boundary, the transmission map can be figured out and used to produce an excellent dehazed image. Experimental results show that our method has competitive effects compared with mainstream underwater single image dehazing methods.

INDEX TERMS Underwater image dehazing, contrast enhancement, image enhancement, scattering removal.

I. INTRODUCTION

Underwater images suffer from lack of contrast and degraded colors due to the absorption and scattering effects. The particles of the water absorb the vast majority of light energy, resulting in dim and blurry images [1]. Usually, degraded underwater images cannot meet the needs of underwater optical vision systems, which leads to the decline in the accuracy of underwater optical target recognition and object detection [2]. It has been proved in [3] that the enhancement of underwater image will contribute to a substantial improvement in the performance of underwater optical vision system. Therefore, researchers keep striving to develop different approaches to enhance the original images for a variety of underwater applications, including object recognition [4], rescue missions, human-made structures inspection, ecological monitoring, sea organisms tracking [5], and real-time navigation [6].

The associate editor coordinating the review of this manuscript and approving it for publication was Sudipta Roy.

Several methods have been presented for single image dehazing, which have achieved excellent enhancing performance in outdoor images. The majority of these methods for outdoor image dehazing are based on the same assumption that the attenuation in the atmosphere is wavelength-independent. In other words, the RGB channels share the same attenuation coefficient. However, unlike those hazy images taken in atmosphere, in underwater images, the attenuation in each color channel is considerably affected by the wavelength of light, which makes the assumption mentioned above fail in underwater environments [7]. Additionally, since the degradation is related to the distance of the object from the camera, this distortion cannot be globally corrected. Thus, the existing atmospheric single image dehazing technology cannot be used for underwater images directly.

Besides, the single image dehazing task is an ill-posed problem with three measurements (the R, G, B values of the input image) and six unknowns (the R, G, B values and transmission of each channel of the output image) [20]. Thus, extra prior or knowledge is required to solve this problem.

This work is licensed under a Creative Commons Attribution 4.0 License. For more information, see https://creativecommons.org/licenses/by/4.0/

Most of the existing underwater single image dehazing methods have noticed the wavelength-dependent attenuation,

and constructed different models to fit the attenuation coefficients in three channels. A variety of priors are proposed to solve the ill-posed problem, such as the underwater dark channel prior (UDCP), the underwater light attenuation prior (ULAP), the histogram distribution prior, the maximum intensity prior (MIP), etc. Although these methods perform well in some cases, they may fail when the imaging condition changes strikingly. This is because these models do not take the correlation between the pixels of an underwater image into consideration.

To robustly enhance the hazy underwater images, in this paper we present a novel method for single underwater image dehazing. Firstly, we improved the background light estimation based on the quad-tree subdivision iteration algorithm by taking the Jerlov water-type [8] into consideration. The improved background light estimation method is verified on images taken under challenging underwater scenes with complex artificial illumination conditions. Afterwards, the color space dimensionality reduction prior was proposed, which is based on a universal observation that the pixels of an underwater image tend to distribute nearby a specific plane in the RGB color space. This prior indicates that the color space can be compressed from the RGB color space to the UV color space by projecting all the pixels onto the plane mentioned above. Via clustering the pixels into several hundred haze-lines in UV color space and carefully setting a haze-free boundary, the transmission map can be calculated accurately and then be used to dehaze the image. Then the Gray-World assumption was used to correct the red channel. Fig. 1 gives a brief flow chart of our method. Besides, for assessing the performance of the proposed method, qualitative and quantitative experiments are conducted, respectively. Experimental results show that the proposed method is characterized by excellent contrast enhancement and dehazing effects.

The contributions of this paper are summarized as follows:

- A novel method for single underwater image dehazing was presented, including the improved background light estimation based on quad-tree subdivision iteration and the transmission map estimation based on the color space dimensionality reduction prior.
- We provided a new approach for the single underwater image dehazing issue by proposing the color space dimensionality reduction prior. This prior allows compressing the color space of an image from 3D to 2D, which reduces the computational complexity while maintaining the accuracy of the transmission estimation.
- The UV color space was proposed, in which the process of color space conversion offsets the phenomenon that attenuation coefficients vary in blue and green channels to a certain degree.
- We introduced the Jerlov water-type [8] and the CIEDE2000 color difference [9] into the quad-tree subdivision iteration algorithm, producing a robust background light estimation method.

The remaining of this paper is organized as follows. In section II, the mainstream image enhancement dehazing methods for underwater images are summarized. Afterwards, a few details about the image formation model (IFM) are presented in section III. The image enhancement method, including the improved background light estimation method and dehazing method based on the color space dimensionality reduction prior, is proposed in section IV, V, and VI. The experimental results are reported in section VII. Finally, conclusion and future work are discussed in section VIII.

II. RELATED WORK

In order to enhance underwater images, numerous methods have been presented, based on hardware and software.

On the one hand, in terms of hardware-based approaches, Schechner and Karpel [10] took two orthogonally polarized photos by adding polarizer to the camera and utilized the partial polarization of light to restore the visibility. Zhang *et al.* [11] obtained the depth information of the image through a multi-camera system and restored the image from the depth map. In [12], multiple images of the same object taken from different known viewpoints were used to estimate attenuation coefficients and recover the scene. These methods have high requirements for the imaging hardware system of the device, so their applicability is limited.

On the other hand, the software-based underwater image enhancement methods have developed rapidly in recent years. Software-based approaches use efficient algorithms to recover underwater images. Typically, these techniques are based on assumptions on different coefficients. Compared to the hardware-based approaches, software-based approaches perform better and cost fewer investment.

Since He *et al.* [13] introduced the Dark Channel Prior (DCP), it has become the most common method for single image dehazing. This method is based on an observation that in a hazy-free image, the value of at least one channel tends to have low intensity. However, due to the excessive attenuation of the red channel, the original DCP method tends to fail in underwater environments. Thus, a variety of DCP variants have emerged recently. Drews *et al.* [14] only considered green and blue channels to produce Underwater Dar Channel Prior (UDCP). Galdran *et al.* [15] employed the inverted red channel to compensate for the loss of information in UDCP due to the abandonment of the red channel. Li *et al.* [16] restored the blue-green channel using the DCP principle and the red channel through the Gray-World assumption theory. However, due to the drawback of DCP, these methods tend to fail when bright objects are involved in images.

In addition to DCP, many other methods also have achieved certain effects. Peng and Cosman [17] developed a depth estimation method for underwater scenes based on image blurriness and light absorption. Carlevaris-Bianco *et al.* [18] presented an image dehazing method based on random Markov fields. Li *et al.* [19] proposed a method to dehaze by minimizing the information loss during transformation.

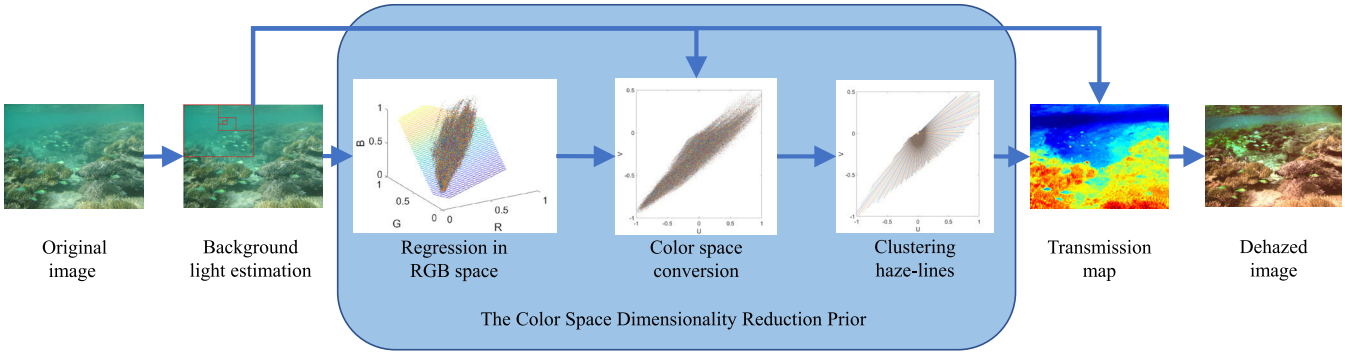

FIGURE 1. The flow chart of proposed method.

These methods showed better performance but tended to fail when artificial illumination is contained. Berman *et al.* [20] exploited the underwater haze-line (UWHL) for underwater image dehazing with new prior knowledge. In his method, the ratio of the attenuation coefficient of each two channel is defined by Jerlov water-types. UWHL showed great performance on dehazing but consumed too much computing resources.

Dehazing method based on machine learning has also been developed recently as the computation power raised rapidly. Ren *et al.* [38] proposed a CNN-based transmission estimation method in 2016, which is named MDCNN, and used synthetic data to train the network. In 2019, they published the improved version of MDCNN [43], which introduced a holistic edge guided network to refine edges of the estimated transmission map. Ren's method inspired other researchers to solve the dehazing task with learning-based approach. Song *et al.* [21] employed the underwater light attenuation prior (ULAP) for underwater image transmission estimation and trained a model with learning-based supervised linear regression. Based on ULAP, they proposed a statistical-based background light estimation models (MABLs) and a new underwater dark channel prior (NUDCP) for estimating a more detailed transmission map [22]. Pan *et al.* [23] developed a CNN, namely Dehaze-Net, to estimate the transmission map and transformed the image into the Hybrid Wavelets and Directional Filter Banks (HWD) domain for de-noising and edge enhancing. Wang *et al.* [24] presented a CNN based network and named it as UIE-Net, which is trained to perform color correction and haze removal. However, due to the lack of ground truth for training the networks, these methods showed greater limitations.

III. THE IMAGE FORMATION MODEL

An underwater image captured by camera can be modeled as a linear superposition of three components [25], [26]: the direct component I_D, which denotes the light reflected by the object; the forward scattering I_{FS}, which causes the light to deviate from its original direction of propagation; the backward scattering I_{BS}, which is formed by the light

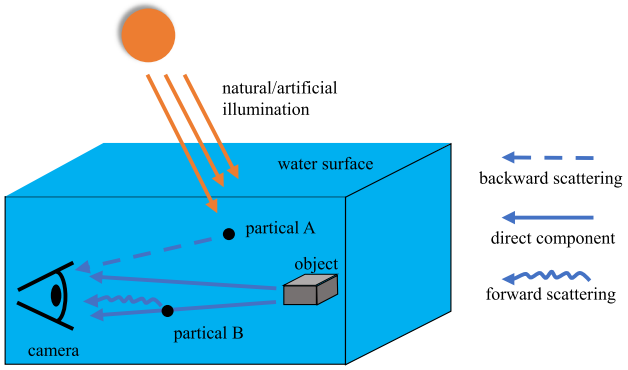

FIGURE 2. The imaging model in underwater environments.

reflected by particles between the object and camera. Fig. 2. shows the imaging model in the underwater environment. This model can be expressed as

$$I = I_D + I_{FS} + I_{BS}. \tag{1}$$

According to [10], most degradation is caused by the backward scattering, meaning the forward scattering can be neglected. The direct and backward scattering components are defined as

$$I_D = Jt, \tag{2}$$

$$I_{BS} = A\,(1 - t)\,, \tag{3}$$

where J represents the object radiance, A denotes the global background light, and t denotes the transmission, which is expressed as

$$t_\lambda = \exp\left(-\beta_\lambda d\right), \tag{4}$$

where t_λ denotes the medium transmission of light of wavelength λ, d is the scene depth, meaning the distance that light travels in water, and β_λ represents the attenuation coefficient of wavelength λ. In addition to wavelength λ, the attenuation coefficient β_λ is also related to the water quality, hydrological environment, and seasonal climate.

In the ocean, the attenuation of red colors can be an order of magnitude larger than the attenuation of blue and green [7].

Therefore, unlike images taken in atmosphere, the transmission t_λ is greatly affected by wavelength λ in underwater environments. Thus, the image formation model shown in (1) can be rewritten as

$$I_c(\boldsymbol{x}) = J_c(\boldsymbol{x})\, t_c(\boldsymbol{x}) + A_c\,(1 - t_c(\boldsymbol{x})), \quad c \in \{R, G, B\}, \quad (5)$$

where bold denotes vectors, $\boldsymbol{x}$ is the pixel coordinate, I_c is the acquired image value of color channel c, $t_c \in [0, 1]$ is the transmission of that color channel, J_c denotes the object radiance that we wish to restore, and A_c represents the global background light of channel c. In (5), the first term on the right side represents the direct component, and the second term represents the backward scattering. This widely used model is called the Image Formation Model (IFM).

It should be noted that in (5), except for the coordinate $\boldsymbol{x}$, all variables are scalars. In other words, the imaging law described in (5) holds in each color channel *independently*.

Our ultimate goal is to recover $J(\boldsymbol{x})$, a haze-free image, from $I(\boldsymbol{x})$, $t(\boldsymbol{x})$, and A. Equation (5) can be rewritten as a medium transmission function:

$$J_c(\boldsymbol{x}) = \frac{I_c(\boldsymbol{x}) - A_c}{t_c(\boldsymbol{x})} + A_c, \quad c \in \{R, G, B\}, \quad (6)$$

In (6), both global background light A and transmission $t(\boldsymbol{x})$ are unknown. In order to solve this ill-posed problem, we proposed novel methods for background light estimation and transmission map estimation, which will be described in detail in sections IV and V.

IV. ROBUST BACKGROUND LIGHT ESTIMATION

The background light A in (6) is usually thought to be the color of the pixels with the furthest distance from the camera in the image. In atmospheric environments, the background light is often estimated as the color of the brightest zone in the image [13]. Such an assumption is usually feasible in the atmosphere, but in underwater conditions, there are two possible problems. First, some large white objects in image are often incorrectly estimated as the background light. Second, the color of water body is usually bluish or greenish, meaning the brightest region in image is definitely not the background light region.

Kim *et al.* [27] proposed a quad-tree iteration subdivision algorithm in hierarchical search of the background light region. Although bright objects may still lead to an incorrect estimation, the quad-tree iteration subdivision with setting a score for each subdivided region has inspired us.

To robustly estimate the background light, we assume that a region with pixels that lie at the infinitive depth with respect to the camera is existed and visible in the image. Such a region should be smooth; meanwhile, its color should be as possible as close to the water body. Mathematically, such a region should have a small variance, and the average color difference between itself and the water body should also be small. Thus, we set a score S_Ω for each subdivided region, shown as

$$S_\Omega = S_\sigma + S_\Delta, \quad (7)$$

where S_Ω denotes the final score of region Ω, S_σ refers to the smoothness of the region. S_Δ represents the color difference between itself and the water body. S_σ in (7) is calculated by

$$S_\sigma = \frac{1}{3} \sum_{c \in \{R,G,B\}} (\overline{I_c(\boldsymbol{x})} - \sigma_c), \quad \boldsymbol{x} \in \Omega, \quad (8)$$

where $I_c(\boldsymbol{x})$ denotes the value of channel c at pixel coordinate $\boldsymbol{x}$, σ_c is the standard deviation of channel c of region Ω. In (8), with introducing $\overline{I_c(\boldsymbol{x})}$, which is the average value of the pixel intensity in the region Ω, as a part of S_σ, our method will give slightly higher scores to brighter regions to avoid getting too dark estimation.

As mentioned above, S_Δ is related to the average color difference between the region and the water body. However, the color of water bodies varies in different water areas and hydrological conditions. In determining the standard water body color, we introduced the Jerlov water-type [8]. Jerlov developed a frequently used classification scheme for oceanic waters based on water clarity. The Jerlov water-types are I, IA, IB, II, and III for open ocean waters, and 1 through 9 for coastal waters. The appearances of a perfect white board at different distances in each kind of water-type are shown in Fig. 3 (a). Considering that the standard colors of different water-types should have significant differences, a group of colors with a distance of 5 meters in Fig. 3 (a) was selected as the standard colors of the water body.

In order to measure the difference between two colors, Sharma *et al.* [9] proposed a color difference calculation method based on perception, namely CIEDE2000. It modifies the non-uniform characteristics of color perception in the CIELAB color space, and is one of the most accurate color difference calculation methods so far. Denoting the CIEDE2000 color difference as E, S_Δ can be expressed as

$$S_\Delta = -\min_{w \in W} (E_{\Omega - w}), \quad \boldsymbol{x} \in \Omega, \quad (9)$$

where W is a set of standard colors of Jerlov water-type, w is the color of a particular water body, and $E_{\Omega-w}$ represents the color difference between the region Ω and water color w.

In the implementation, the two parts of scores, S_σ and S_Δ, should have different weights in different stages of the quad- tree iteration. More specifically, in the earlier iteration rounds, S_Δ is supposed to have a larger weight than S_σ so that the regions which obviously do not contain the water body can be discarded quickly. Conversely, in the later iteration rounds, S_σ should have a larger weight to help us find a smoother region as the final background light estimation region. Therefore, we finally fix the score S_Ω defined in (7) as

$$S_\Omega = S_\sigma \log_{10}(\eta r) + S_\Delta, \quad (10)$$

where r represents the round of iterations, η is a controlling factor used to control the dropping speed of weight of S_Δ, usually set as 2 or 3.

After the score of each region is calculated according to (10), the region with the best score will be selected to

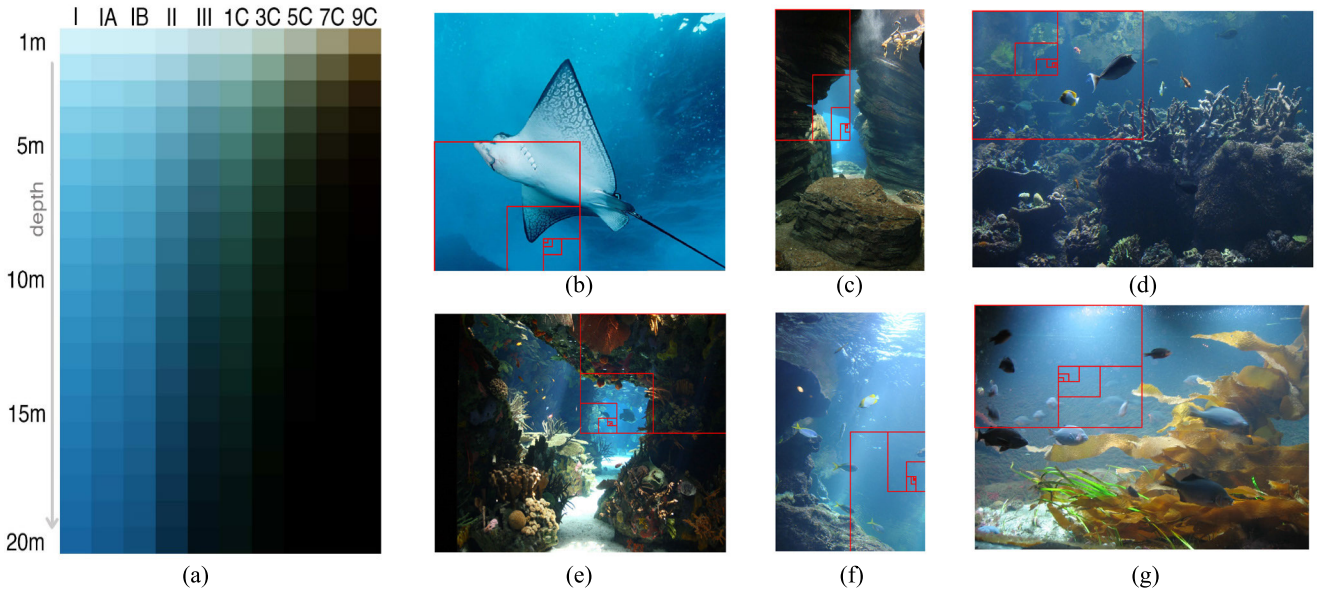

FIGURE 3. (a) RGB simulation of the appearance of a perfect white surface viewed in 1-20m depth in different water-types [8], the appearances at a distance of 5 meters are selected as standard colors of background light. Image (b-g) are examples of our background light estimation method, which illustrate that our method has a natural immunity to large bright zones and works well even under complex artificial illumination conditions.

continue the quad-tree subdivision iteration until the size of the region is smaller than a preset threshold. The average pixel intensity of the latest region can be utilized as the estimated background light. As shown in Fig. 3, even in images with bright objects or complex illumination conditions, our background light estimation method shows excellent adaptability.

V. THE COLOR SPACE DIMENSIONALITY REDUCTION PRIOR

In this section, we will introduce the color space dimensionality reduction prior in detail and explain it mathematically.

A. THE PRIOR AND VALIDATION

Since the attenuation coefficient β_λ of the red channel is several orders of magnitude greater than that of the blue and green channels under water [39], according to (4), the transmission of the red channel t_R will attenuate faster than that of the blue and green channels (t_B and t_G) as the scene depth d increases. This will cause the direct component of the red channel of the image to decrease, the backscattering component to increase, and the value of the red channel to drift rapidly to A_R, referring to (2), (3), and (5).

Based on this inference, we observed the pixels distribution of a large number of underwater images in the RGB color space and obtained an interesting fact. Observation showed that in most underwater images, all the pixels tend to distribute nearby a specific plane in RGB color space. This phenomenon is named color space dimensionality reduction.

To validate this observation, we tried to find the plane where the pixels in each image tend to distributed nearby by simple linear regression, and then projected all the pixels of an image onto this regressed plane. It turned out that the process of projecting did not lead to any unacceptable excessive color shift.

Based on the analysis above, we proposed the color space dimensionality reduction prior (abbreviated as **CSDRP**): Pixels of most underwater images tend to be distributed nearby a specific plane in RGB color space. Projecting these pixels on this plane does not cause excessive color drift.

The **CSDRP** was validated on the UIEBD Dataset [28], which includes 890 original raw underwater images. The root mean square error (RMSE) and R-squared [29] were selected to measure how well the model fits the data. Additionally, the Peak Signal to Noise Ratio (PSNR) between the original and projected image was chosen to measure the impact of the projection process on the image.

The average RMSE and adjusted R-squared on this dataset were 0.0552 and 0.7390, respectively. The PSNR of the projected images, compared to the original ones, were high, ranged from 28.61dB to 100.34dB, and shared an average of 48.02dB. Validation results show that the differences between the projected images and the original ones are relatively small, so it is feasible to use the projected image to estimate the transmission. Fig. 4 shows the validation experimental results.

B. MATHMATICAL EXPLANATION

The **CSDRP** points out that the pixels of most underwater images tend to be distributed nearby a specific plane in RGB space. This can be explained mathematically as following part in this section.

Note (4), the medium transmission is determined by two factors, i.e., the attenuation coefficient β_λ and the depth d.

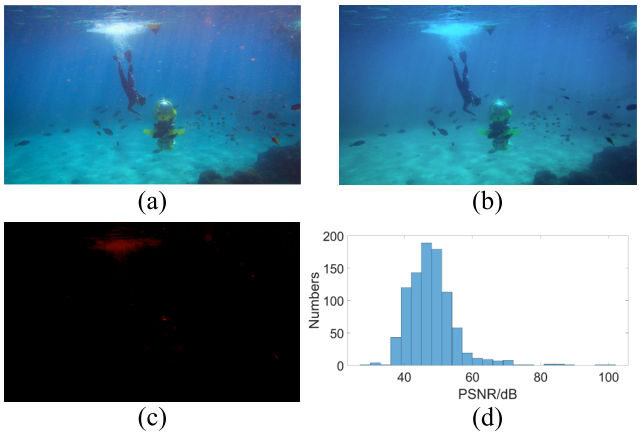

FIGURE 4. Prior validation. (a) and (b) show the example with the *worst* PSNR, before and after projecting. (c) shows the absolute difference between (a) and (b). (d) is a PSNR histogram of the quantization errors on the UIEBD dataset.

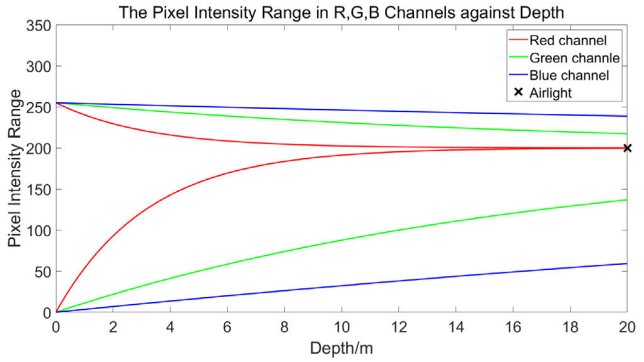

FIGURE 5. The pixel intensity range in R, G, B, channels against depth. The areas which are surrounded by curves with the same color represent the distributable ranges of pixel intensity in the correspond channel. Here, taking Jerlov water-type as an example, the attenuation coefficients of three channels are $\beta_R = 0.3123$, $\beta_G = 0.0577$, and $\beta_B = 0.0176$ [42], and the transmission is calculated using (12).

The transmission of R, G, B channel can be expressed as

$$t_c = \exp\left(-\beta_c d\right), \quad c \in \{R, G, B\}. \tag{11}$$

According to [40] and [41], λ_R, λ_G, and λ_B are 620nm, 540nm, and 450nm, respectively, in general water. Taking Jerlov water-type I as an example, the attenuation coefficients of such wavelengths are $\beta_R = 0.3123$, $\beta_G = 0.0577$, and $\beta_B = 0.0176$ [42]. Now the transmission t becomes a univariate function with respect to the depth d:

$$\begin{cases} t_R = \exp\left(-0.3123d\right), \\ t_G = \exp\left(-0.0577d\right), \\ t_B = \exp\left(-0.0176d\right). \end{cases} \tag{12}$$

In accordance to (5), as the depth increases, the pixel intensity I_c will gradually converge to the background light point A_c. However, due to the different transmission functions of the RGB color channels described in (12), they would converge at different rates. Fig. 5 demonstrates the convergency-depth relationship, where the transmission is calculated using (12).

As shown in Fig. 5, with the depth increasing, the pixel intensity of red channel converges much faster than those of green and blue channels. According to (5) and (12), In the Jerlov water-type I, when the depth reaches 5 meters, the red channel only retains 20.98% of the scene radiance (J_c) information. When the depth reaches 10m, this number drops to 4%. When the depth reaches 20m, more than 99.8% of the information in the red channel is replaced by the background light A_R, meanwhile 31.54% for green channel and 70.33% for blue channel object radiance is retained. Remind, these numbers are calculated by simulation under Jerlov water-type I, and in other water-types with even poorer visibility, the attenuation of the red channel is more serious.

When the scene radiance component of the red channel J_R decreases with increasing depth, the pixel intensity of the red channel will be limited to a small range near A_R. At the same time, the blue and green channels still retain a large amount of scene radiance information J_B and J_G, which results the red channel is compressed into a flat plane in the RGB space.

Therefore, in underwater images, only those pixels with a small depth still retain the red channel information of the source pixels. Conversely, the pixels with bigger depth tend to be distributed near the plane $R = A_R$ in RGB color space. That is, the phenomenon of color space dimensionality reduction of the underwater images.

VI. HAZE REMOVAL

A. COLOR SPACE CONVERSION

According to the **CSDRP**, the fitted plane can be obtained by simple linear regression in RGB color space. This regressed plane can be expressed as

$$aR + bG + cB + d = 0, \tag{13}$$

where a, b, c, and d are the regression coefficients obtained in linear regression.

All pixels, together with the estimated background light A, can be projected onto this plane by

$$\begin{cases} R_p = \dfrac{\left(b^2 + c^2\right) R_0 + a\left(bG_0 + cB_0 + d\right)}{a^2 + b^2 + c^2}, \\ G_p = \dfrac{\left(a^2 + c^2\right) G_0 + b\left(aR_0 + cB_0 + d\right)}{a^2 + b^2 + c^2}, \\ B_p = \dfrac{\left(a^2 + b^2\right) B_0 + c\left(aR_0 + bG_0 + d\right)}{a^2 + b^2 + c^2}. \end{cases} \tag{14}$$

Since all pixels have been projected onto this plane, the color space is conversed from the 3D RGB color space to a 2D one, which is called the UV color space in this paper. Specify that the projection of the positive directions of the G and B axes on the UV color space as the positive directions of the U and V axes, respectively. Then the UV coordinate of

each pixel can be calculated by

$$\begin{cases} U_p = G_p\sqrt{1+\left(\frac{b}{a}\right)^2}, \\ V_p = B_p\sqrt{1+\left(\frac{c}{a}\right)^2}. \end{cases} \tag{15}$$

In order to facilitate subsequent calculations, we set the estimated background light point as the origin and translate the coordinates by

$$\begin{cases} U = U_p - A_U, \\ V = V_p - A_V. \end{cases} \tag{16}$$

where A_U and A_V denote the UV coordinate of the projected background light point.

After mapping the pixels to the UV color space, the next step is to estimate the transmission map.

B. TRANSMISSION ESTIMATION

Since the process of converting RGB coordinates to UV coordinates is a linear transformation process, the imaging law described in (5) still holds in UV space.

As described in [30], the number of distinct colors is several orders of magnitude smaller than the number of pixels in the image, and a haze-free image can be clustered into about 500 different colors. Therefore, the pixels of a haze-free image can be clustered into groups nearby their cluster centers in RGB color space. However, referring to (5), these groups will be stretched in hazy images, meaning the color of the pixels with farther depth and more haze will be closer to the background light point. Specially, the pixels at infinite depth (at which the transmission is 0) will completely lose their original color and be replaced by the color of the background light point. On the contrary, pixels at which the transmission is 1 are regarded as the haze-free point. In summary, the pixels with haze will be "pushed" from its original color to the background light geometrically in hazy images [31].

Therefore, the pixels that are clustered into the same color group will be distributed on a straight line formed by the background light point and the haze-free point of this color group. This line is called haze-line [32].

As we have set the background light point as the origin, the haze-lines of all color cluster will become a set of lines radiating from the origin to the surroundings in UV color space. Here, we rewrite the UV coordinates (U, V) of the pixels as polar coordinates form (ρ, θ).

According to (5), the transmission is distributed linearly on haze-lines [32]. If we can find a haze-free point on each haze-line, the transmission of each point on the line can be calculated by

$$\hat{t_I} = \frac{\rho_I}{\rho_{HF}^l}, \quad I \in l, \tag{17}$$

where t_I denotes the transmission of point I, ρ_I and ρ_{HF}^l refer to the Euclidean distance from the background light point to point I and to the haze-free point, respectively.

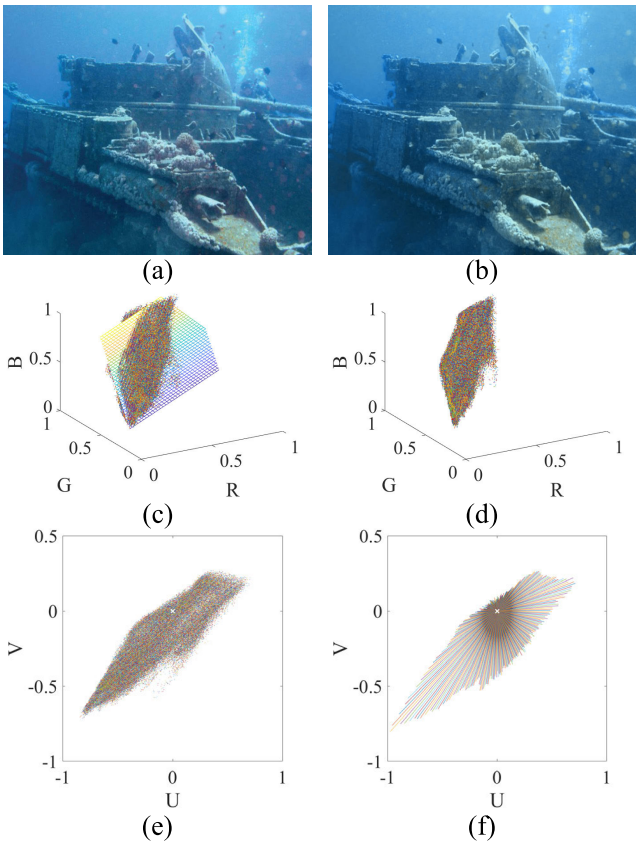

FIGURE 6. (a) Original image. (b) Projected image. (c) The distribution of original image pixels in RGB color space and the fitted plane. (d) The distribution of projected image pixels in RGB color space. (e) The distribution of projected image pixels in UV color space. (f) The clustered haze-lines which are connected by the background light point and haze-free point of a certain haze-line. Here, 360 haze-lines are clustered in (f).

In [32], the haze-free point is simply estimated as the furthest pixel on each haze-line, in which the noises may lead to some outlier interference. It can be seen in Fig. 6 (e) that a few outlier pixels lie below the background light point. Without correction, the haze-free points of the haze-lines down below will be wrongly estimated further. Thus, in proposed method, the haze-free point is estimated by

$$\begin{cases} \rho_{HF}^l = k(\max(\rho_I) + \overline{\rho_I}) \\ \theta_{HF}^l = \overline{\theta_I}, \end{cases} \quad I \in l, \tag{18}$$

where $\rho_{HF}^l, \theta_{HF}^l, \rho_I, \theta_I$ are the polar coordinates of the haze-free point and the point I in the UV color space, respectively. k is a multiplier factor used for reducing outlier interference, usually set as 2/3. According to (17) and (18), we can calculate the transmission of each pixel by

$$\hat{t_I} = \frac{\rho_I}{k\left(\max\limits_{I\in l}(\rho_I) + \overline{\rho_I}\right)}, \quad I \in l. \tag{19}$$

It is essential to note that the estimated haze-free point is sometimes close to the background light point in UV space. As shown in Fig. 6 (f), there are dozens of haze-lines which

are strikingly shorter than the others, especially in the direction of the top-left of the background light point. The pixels on such haze-lines distribute nearly to the background light point, colored close to the color of water body, and are supposed to value relatively small transmission. On these haze-lines, the haze-free point estimated by (18) is inaccurate, and the transmission values of the pixels will be overestimated. Thus, we modify the transmission on these haze-lines by

$$\hat{t_I} = \frac{\rho_I}{\max\limits_l \left(\rho^l_{HF}\right)}, \quad if\ \rho^l_{HF} < \beta \max_l \left(\rho^l_{HF}\right),\ I \in l, \tag{20}$$

where $\max\limits_l \left(\rho^l_{HF}\right)$ denotes the maximum value of radius ρ among all estimated haze-free points, β is a constant used to control how far the nearest haze-free point is, which is usually set less than 0.2. In (20), the denominator is set as $\max\limits_l \left(\rho^l_{HF}\right)$, this is considered in two aspects: On the one hand, as mentioned above, these pixels are supposed to have a small transmission, so their corresponding haze-free points should have bigger radius. On the other hand, generally speaking, the haze-line with the largest radius contains more pixels, and the estimation of haze-free point based on these pixels is more accurate.

C. HAZE REMOVAL

The transmission map calculated by the above method first requires to be refined by a guided filter to remove ''pixel holes'' in the transmission map before image restoration.

Since the transformation from RGB space to UV space is only a linear transformation, the transmission we obtained in UV space can be used directly for the image restoration process described in (6) only in green and blue channels without any spatial transformation:

$$J_c(\boldsymbol{x}) = \frac{I_c(\boldsymbol{x}) - \hat{A_c}}{\hat{t}(\boldsymbol{x})} + \hat{A_c}, \quad c \in \{G, B\}. \tag{21}$$

To avoid excessive restoration, we set the minimum transmission as 0.1.

As the transmission characteristics of red channel underwater are different from those of blue and green channels, the estimated transmission map is usually difficult to restore a clear red channel image. Fortunately, the Gray-World assumption provided us an approach to correct the red channel. The assumption indicates that the average intensity of R, G, B channels tend to be the same value $\overline{Gray}$. It can be defined as

$$(\overline{I_R} + \overline{I_G} + \overline{I_B})/3 = \overline{Gray}, \tag{22}$$

where I_R, I_G, I_B indicate the pixels intensity of original image. Denoting the pixels intensity of dehazed image as J_R, J_G, J_B, the same assumption holds as

$$(\overline{J_R} + \overline{J_G} + \overline{J_B})/3 = \overline{Gray}. \tag{23}$$

According to (22) and (23), the compensation coefficient δ can be calculated as

$$\delta = \overline{J_R}/\overline{I_R}. \tag{24}$$

Then the recovered red channel can be obtained by

$$J_R(\boldsymbol{x}) = \delta I_R(\boldsymbol{x}). \tag{25}$$

VII. EXPERIMENTAL RESULTS

In order to evaluate the performance of the proposed method on the dehazing task, qualitative and quantitative comparison are carried out, respectively.

The methods used for comparisons include MIP method [18], Underwater Dark Channel Prior (UDCP) method [14], Blue-Green Channels Dehazing and Red Channel Correction (BGCD&RCC) method [16], Image Blurriness and Light Absorption method (IBLA) [17], Underwater Light Attenuation Prior (ULAP) method [21], Statistical Model of BL and Optimization (SMBLO) method [22], Dehaze-Net method [23], Multi-scale Dehazing Convolutional Neural Network (MDCNN) method [38], Minimum Information Loss (MIL) method [19], and Underwater Haze-line (UWHL) method [20]. These selected methods for comparison not only include traditional classical underwater dehazing methods based on the IFM (i.e., UDCP, MIP, and MIP), but also include methods which are proposed in recent years, based on deep learning, statistical models or new optical priors (i.e., IBLA, ULAP, SMBLO, and Dehaze-Net). Additionally, since our proposed method is inspired by the Haze-line method [32], it was also added into our experiments.

The code of SMBLO, Dehaze-Net, MIL, and UWHL are available and released by authors on Github, and the code of MIP, UDCP, BGCD&RCC, IBLA, and ULAP used for comparison experiments are provided by Wang *et al.* in [33].

In total, 1009 images were implemented on each selected method, most of which are collected from the datasets in [20], [28], and others are collected from the Internet. All methods are implemented on a Windows 10 PC with an Intel i7-8550U CPU and an Nvidia GeForce MX150 GPU, running on MATLAB R2019b and Anaconda 3 with Python 3.7.

A. QUALITATIVE EXPERIMENTAL RESULTS

Fig. 7 demonstrates parts of the qualitative comparison results. SMBLO, MIL, and ULAP show limited dehazing performance, especially in areas marked by red rectangles. Dehaze-Net shows considerable dehazing ability, especially in image (b), but overall reduces the saturation of the images, and the effectiveness of dehazing in the areas with a large depth is not strong enough. IBLA shows an unsatisfactory dehazing result unless the image exposure is reduced to an unacceptable level, which will result in loss of dark details, e.g. image (c) and (e). UDCP shows a good dehazing effect, but it also has similar exposure problems as IBLA. UWHL shows considerable performance on color restoration, but in terms of dehazing, the effect is not apparent enough. MIP has impressive dehazing capabilities, but in the images (b), some areas are overexposed, which may cause the loss of image details. Similarly, in image (a) and (d), some areas are underexposed. MDCNN has a certain performance on

FIGURE 7. Part of the qualitative experimental results. Best viewed on high-resolution display with zoom-in.

dehazing, but there are underexposure problems in images (b) and (d), resulting in the loss of image details. Haze-line, whose method inspired us a lot, does not show the excellent performance that it shows in atmosphere due to the inaccurate background light estimation. Noticing the areas surrounded by the red rectangles in the images, compared with other

TABLE 1. Quantitative experimental results.

Method	UCIQE	UIQM	UIConM	BRISQUE*	PCQI($\times 10^4$)	Avg. Rank*
SMBLO [22]	27.4650(9)	6.2602(5)	0.6102(10)	24.8410(7)	**0.8412(1)**	6.4
IBLA [17]	31.2180(4)	4.8187(10)	0.5973(11)	29.0067(10)	0.5656(10)	9.0
ULAP [21]	29.7991(6)	6.3423(4)	0.7041(4)	**22.6973(1)**	0.7962(3)	3.6
MIL [19]	26.2532(11)	6.4617(3)	0.6946(5)	23.4241(2)	0.7276(6)	5.4
UDCP [14]	27.3695(10)	5.4719(9)	0.6241(8)	23.6387(4)	0.3327(11)	8.4
MIP [18]	29.7155(7)	6.1723(6)	0.6400(7)	25.7725(9)	0.7769(4)	6.6
DEHAZE-NET [23]	27.5543(8)	6.9693(2)	0.8660(2)	29.3160(11)	0.7617(5)	5.6
MDCNN [38]	30.9567(5)	5.7971(8)	0.7738(3)	23.6398(5)	0.6001(9)	6.0
Haze-line [32]	31.7933(3)	2.5526(11)	0.6166(9)	24.2918(6)	0.7219(7)	7.2
UWHL [20]	**32.7735(1)**	6.1298(7)	0.6760(6)	24.8685(8)	0.6716(8)	6.0
Ours	32.0818(2)	**7.0745(1)**	**0.9184(1)**	23.6225(3)	0.8384(2)	**1.8**

Terms with * are the smaller, the better. The number in brackets refers to the ranking 1-9 of a method on the metric. The values in bold represent the best results.

methods, our proposed method has predominant improvement in contrast and visibility in these areas. We also noticed that although our method improves the visibility and contrast of the images and shows impressive performance on dehazing task, it also introduces unexpected stratification in water zones, e.g. image (a). In addition, our method does not seem to suppress forward scatter enough, resulting in blurred object edges. In summary, for qualitative experiments, our proposed dehazing method is more robust than other methods, and the improvement in contrast and visibility is more prominent.

Terms with $*$ are the smaller, the better. The number in brackets refers to the ranking 1-9 of a method on the metric. The values in bold represent the best results.

B. QUANTITATIVE EXPERIMENTAL RESULTS

In quantitative experiments, since it is impossible to obtain medium-free *in situ* images in underwater environments, the comparisons are based on non-reference image quality metrics and contrast quality assessment indexes.

Recently, an underwater color image quality evaluation metric (UCIQE) [34] has been proposed by Yang and Sowmya for quantifying the non-uniform color cast, blurring, and low contrast of underwater images. The higher UCIQE values indicate the image has a better balance among the chroma, saturation, and contrast. Panetta and Gao [35] have developed three underwater image quality metrics: UICM on color, UISM on sharpness, and UIConM on contrast. By assigning carefully calculated weights to the three metrics, the underwater image quality metric (UIQM) is finally obtained to characterize the underwater quality. Moreover, as the contrast is considered as a better evaluation indicator in dehazing problem, UIConM is also chosen to measure the contrast quality of an image. Both UIQM and UIConM are the higher, the better. The Blind/Referenceless Image Spatial Quality Evaluator (BRISQUE) [36] is predicted by a support vector regression (SVR) model trained on an image database which contains images with known distortion (e.g., artifacts, blurring, and noise) and the pristine versions of the distorted images. A smaller BRISQUE score indicates better perceptual quality. Additionally, Wang *et al.* [37] proposed a metric based on an adaptive representation of local patch structure for providing accurate predictions on the human perception of contrast variations, namely PCQI. A higher PCQI value indicates the image has better contrast quality.

Table 1 summarizes the average UCIQE, UIQM, UIConM, BRISQUE, and PCQI results on the whole dataset mentioned above. In Table 1, the values in bold represent the best results. As shown in Table 1, although our dehazing method does not rank first in three of five quantitative experimental indicators, it can still rank in the top three among all the indicators with a small gap from the first. Moreover, compared to any one of the selected comparison methods, our dehazing method can outperform them in at least four of the five quantitative indicators.

More specifically, our dehazing method stands out among the compared methods in terms of UIConM, indicating that our dehazing method shows excellent performance on improving the contrast of the image. Since PCQI is a local patch-based objective quality assessment metric, it is more sensitive to the contrast change of the main object that occupying a larger area in image. Quantitative experimental results tell us that SMBLO is better than the proposed method at improving the contrast of the main objects in the image. The qualitative experiment results shown in Fig. 7 also confirm this. For example, the main object in image (a) and (b) share a bright appearance in the results of SMBLO. However, the second-ranked PCQI value still means that our method significantly improves the perceptional contrast of the original image. The reason our method ranks only third in terms of BRISQUE is because BRISQUE is a perceptual-based

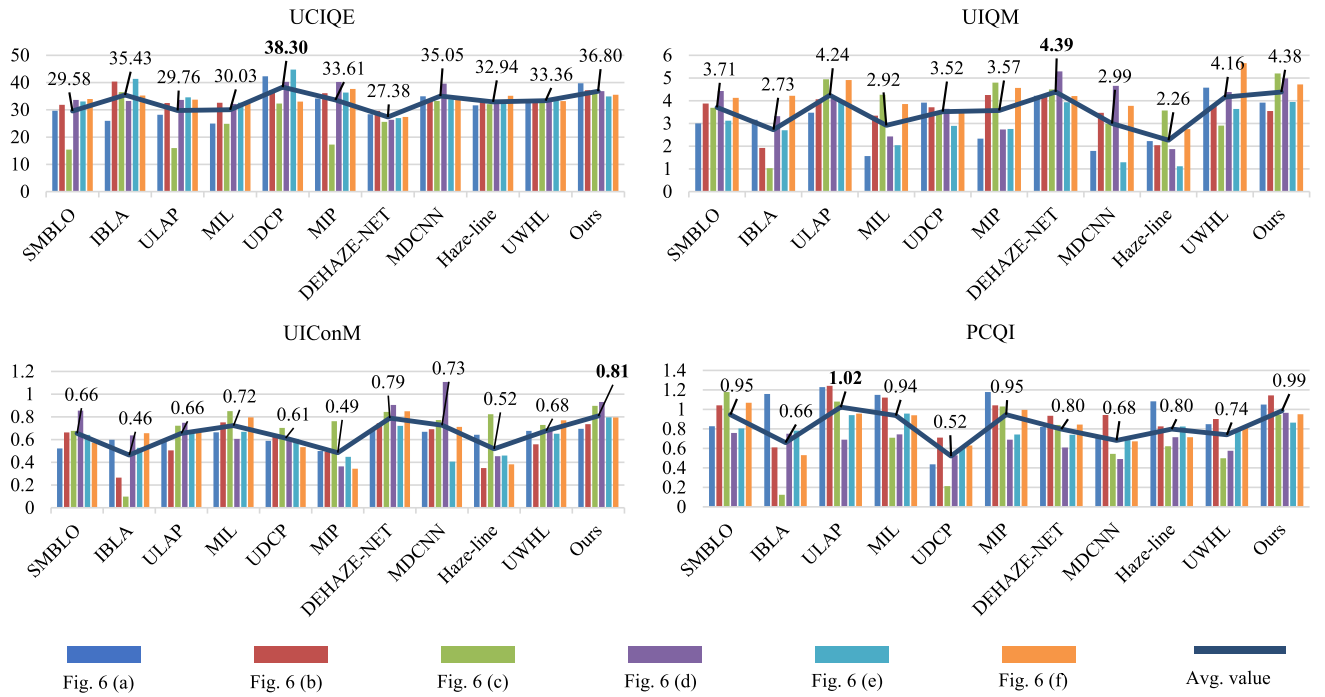

FIGURE 8. Quantitative experimental results for images in Fig. 7. Figure (a)-(d) demonstrate the UCIQE, UIQM, PCQI, and UIConM of examples showed in Fig. 7, respectively. Polylines and values indicate the average of these examples. The values in bold represent the best results.

metric, and in our method, the dehazing process will greatly improve the contrast of the image, which will make the image look dazzling, perceptually. Additionally, in terms of UCIQE and UIQM, the metrics which are specifically designed for underwear images, our dehazing method also performs well, ranking second in UCIQE and first in UIQM, which means the underwater images restored by our method are of better quality. It is essential to note that the UCIQE metric, which is a linear combination of chroma, saturation, and contrast, has the greatest weight in chroma. However, the proposed method does not perform well enough in color restoration, so it only ranks second in UCIQE. In summation, compared to other selected comparison methods, our proposed method has better robustness and achieve specific high scores in various quality metrics, which means that our method can indeed restore high quality underwater images from the hazy ones.

Besides, the quantitative experimental results for examples in Fig. 7 are displayed in Fig. 8. It turned out that the perceptual qualitative experimental results are not consistent with the quantitative ones. The UDCP method, which showed underexposure problems in qualitative experiments, ranked first on the UCIQE metric but performed unevenly in the five test images. The proposed method has the second-ranked mean in this indicator, and is relatively stable overall. On the UIQM index, the proposed method scored above 3.5 on all five examples, ranking second of nine. In addition, the first-ranked UIConM and BRISQUE also proved that the proposed method improves the contrast quality of the image while maintaining a fairly high image perception quality.

VIII. CONCLUSION AND FUTURE WORK

In this paper, we introduced an underwater image dehazing method, which includes a modified Quad-tree-subdivision-based under-water background light estimation algorithm and a **CSDRP**-based underwater image dehazing algorithm. The background light can be accurately estimated by introducing a region score, which take the smoothness and the color difference into account simultaneously. Then we proposed the color space dimensionality reduction prior, the **CSDRP**, which is based on a universal observation that all the pixels tend to distribute nearby a specific plane in RGB color space in most underwater images. With the **CSDRP**, we can converse the color space of the image from RGB color space to UV color space, figure out the transmission map, and then dehaze the image easily. Extensive experiments demonstrate that our dehazing results are characterized by relatively high contrast, improved visibility, and more details. Meanwhile, quantitative experimental results indicate that underwater images with high quality can be restored with our method.

Despite the excellent performance, our method nevertheless has some limitations and shortcomings. First, we noticed that in some of the images recovered by our algorithm, some artifacts appeared at the water-land junction, which is because our algorithm did not suppress the forward scattering well. Second, our proposed method may sometimes introduce unexpected stratification in water zones, which is yet to be improved. For future work, we intend to address the issues mentioned above.

APPENDIX

The pseudo-code of background light estimation and haze removal are shown as following.

Algorithm 1 Background Light Estimation

Input: $I(\boldsymbol{x})$, threshold
Output: $\boldsymbol{A}$
1: Subdivide I into 4 regions $\Omega_1, \Omega_2, \Omega_3, \Omega_4$
2: **for** each region Ω_i **do**:
3: $S_\sigma := \frac{1}{3} \sum_{c\epsilon\{R,G,B\}} (\overline{I_c(\boldsymbol{x})} - \sigma_c), \boldsymbol{x} \in \Omega_i$
4: $S_\Delta := -\min_{w\in W} (E_{\Omega-w}), \boldsymbol{x} \in \Omega_i$
5: $S_{\Omega_i} := S_\sigma \log_{10}(\eta r) + S_\Delta$
6: **end for**
7: Select the region with the best score S_{Ω_i}, denote the region as Ω_{out}
8: **while** size of Ω_{out} > threshold **do**:
9: **repeat** step 1 to step 7
10: $\mathbf{A} := \overline{\Omega_{out}(x)}$

Algorithm 2 Haze Removal

Input: $I(\boldsymbol{x}), \boldsymbol{A}$
Output: $J(\boldsymbol{x})$
1: Find the plane in RGB space by linear regression
2: Converse $I, \boldsymbol{A}$ from the RGB space to the UV space, remind as I_p, A_p
3: Take point A_p as the origin and rewrite all coordinates to polar coordinates (ρ, θ)
4: Cluster the pixels with close θ values into a Haze-line l
5: **for** each Haze-line l **do**:
6: **for** each pixel I on Haze-line l **do**:
7: **if** $\max_{I\in l}(\rho_I) > 0.2 \max_{l}(\max_{I\in l} \rho_I)$:
8: $\hat{t_I} := \frac{\rho_I}{k(\max_{I\in l}(\rho_I)+\overline{\rho_I})}$
9: **else**:
10: $\hat{t_I} := \frac{\rho_I}{(\max_{l}(\max_{I\in l} \rho_I))}$
11: **end for**
12: **end for**
13: **for** each pixel $\boldsymbol{x}$ **do**:
14: $J_c(\boldsymbol{x}) := \frac{I_c(\boldsymbol{x})-\boldsymbol{A}_c}{\hat{t}(\boldsymbol{x})} + \hat{A}_c, c \in \{G, B\}$
15: **end for**
16: Use the Gray-World assumption to recover $J_R(\boldsymbol{x})$

REFERENCES

[1] H. Lu, Y. Li, X. Xu, J. Li, Z. Liu, X. Li, J. Yang, and S. Serikawa, "Underwater image enhancement method using weighted guided trigonometric filtering and artificial light correction," *J. Vis. Commun. Image Represent.*, vol. 38, pp. 504–516, Jul. 2016.
[2] J. P. Oakley and B. L. Satherley, "Improving image quality in poor visibility conditions using a physical model for contrast degradation," *IEEE Trans. Image Process.*, vol. 7, no. 2, pp. 167–179, Feb. 1998.
[3] Y. Xu, J. Wen, L. Fei, and Z. Zhang, "Review of video and image defogging algorithms and related studies on image restoration and enhancement," *IEEE Access*, vol. 4, pp. 165–188, 2016.
[4] K. Kim, J. Kim, S. Kang, J. Kim, and J. Lee, "Object recognition for cell manufacturing system," in *Proc. 9th Int. Conf. Ubiquitous Robots Ambient Intell. (URAI)*, Nov. 2012, pp. 512–514.
[5] H. Lu, T. Uemura, D. Wang, J. Zhu, Z. Huang, and H. Kim, "Deep-sea organisms tracking using dehazing and deep learning," *Mobile Netw. Appl.*, pp. 1–8, Oct. 2018. [Online]. Available: https://link.springer.com/article/10.1007%2Fs11036-018-1117-9#citeas
[6] D. J. Lee, S. Redd, R. Schoenberger, X. Xu, and P. Zhan, "An automated fish species classification and migration monitoring system," in *Proc. IECON 29th Annu. Conf. IEEE Ind. Electron. Soc.*, Nov. 2003, pp. 1080–1085.
[7] C. Mobley, *Light and Water: Radiative Transfer in Natural Waters*. San Diego, CA, USA: Academic, 1994.
[8] N. Jerlov, *Marine Optics*. Amsterdam, The Netherlands: Elsevier, 1976.
[9] G. Sharma, W. Wu, and E. N. Dalal, "The CIEDE2000 color-difference formula: Implementation notes, supplementary test data, and mathematical observations," *Color Res. Appl.*, vol. 30, no. 1, pp. 21–30, Feb. 2005.
[10] Y. Y. Schechner and N. Karpel, "Recovery of underwater visibility and structure by polarization analysis," *IEEE J. Ocean. Eng.*, vol. 30, no. 3, pp. 570–587, Jul. 2005.
[11] S. Zhang, J. Zhang, S. Fang, and Y. Cao, "Underwater stereo image enhancement using a new physical model," in *Proc. IEEE Int. Conf. Image Process. (ICIP)*, Oct. 2014, pp. 5422–5426.
[12] A. Yamashita, M. Fujii, and T. Kaneko, "Color registration of underwater images for underwater sensing with consideration of light attenuation," in *Proc. IEEE Int. Conf. Robot. Autom.*, Apr. 2007, pp. 4570–4575.
[13] K. He, J. Sun, and X. Tang, "Single image haze removal using dark channel prior," in *Proc. IEEE Conf. Comput. Vis. Pattern Recognit.*, Miami, FL, USA, Sep. 2009, pp. 1956–1963.
[14] P. Drews Jr, E. do Nascimento, F. Moraes, S. Botelho, and M. Campos, "Transmission estimation in underwater single images," in *Proc. IEEE Int. Conf. Comput. Vis. Workshops*, Dec. 2013, pp. 825–830.
[15] A. Galdran, D. Pardo, A. Picón, and A. Alvarez-Gila, "Automatic red-channel underwater image restoration," *J. Vis. Commun. Image Represent.*, vol. 26, pp. 132–145, Jan. 2015.
[16] C. Li, J. Quo, Y. Pang, S. Chen, and J. Wang, "Single underwater image restoration by blue-green channels dehazing and red channel correction," in *Proc. IEEE Int. Conf. Acoust., Speech Signal Process. (ICASSP)*, Mar. 2016, pp. 1731–1735.
[17] Y.-T. Peng and P. C. Cosman, "Underwater image restoration based on image blurriness and light absorption," *IEEE Trans. Image Process.*, vol. 26, no. 4, pp. 1579–1594, Apr. 2017.
[18] N. Carlevaris-Bianco, A. Mohan, and R. M. Eustice, "Initial results in underwater single image dehazing," in *Proc. Oceans MTS/IEEE Seattle*, Sep. 2010, pp. 1–8.
[19] C.-Y. Li, J.-C. Guo, R.-M. Cong, Y.-W. Pang, and B. Wang, "Underwater image enhancement by dehazing with minimum information loss and histogram distribution prior," *IEEE Trans. Image Process.*, vol. 25, no. 12, pp. 5664–5677, Dec. 2016.
[20] D. Berman, D. Levy, S. Avidan, and T. Treibitz, "Underwater single image color restoration using haze-lines and a new quantitative dataset," *IEEE Trans. Pattern Anal. Mach. Intell.*, early access, Mar. 2, 2020, doi: 10.1109/TPAMI.2020.2977624.
[21] W. Song, Y. Wang, D. Huang, and D. Tjondronegoro, "A rapid scene depth estimation model based on underwater light attenuation prior for underwater image restoration," *Adv. Multimedia Inf. Process. PCM*, 2018, pp. 678–688.
[22] W. Song, Y. Wang, D. Huang, A. Liotta, and C. Perra, "Enhancement of underwater images with statistical model of background light and optimization of transmission map," *IEEE Trans. Broadcast.*, vol. 66, no. 1, pp. 153–169, Mar. 2020.
[23] P. Pan, F. Yuan, and E. Cheng, "Underwater image de-scattering and enhancing using dehazenet and hwd," *J. Mar. Sci. Technol. (Taiwan)*, vol. 26, pp. 531–540, Jan. 2018.
[24] Y. Wang, J. Zhang, Y. Cao, and Z. Wang, "A deep CNN method for underwater image enhancement," in *Proc. IEEE Int. Conf. Image Process. (ICIP)*, Sep. 2017, pp. 1382–1386.
[25] B. McGlamery, "A computer model for underwater camera systems," *Proc. SPIE*, vol. 208, pp. 221–231, Jan. 1979.
[26] J. S. Jaffe, "Computer modeling and the design of optimal underwater imaging systems," *IEEE J. Ocean. Eng.*, vol. 15, no. 2, pp. 101–111, Apr. 1990.
[27] J.-H. Kim, W.-D. Jang, J.-Y. Sim, and C.-S. Kim, "Optimized contrast enhancement for real-time image and video dehazing," *J. Vis. Commun. Image Represent.*, vol. 24, no. 3, pp. 410–425, Apr. 2013.
[28] C. Li, C. Guo, W. Ren, R. Cong, J. Hou, S. Kwong, and D. Tao, "An underwater image enhancement benchmark dataset and beyond," *IEEE Trans. Image Process.*, vol. 29, pp. 4376–4389, Nov. 2020.

[29] A. Colin, F. A. G. Windmeijer, H. Gramajo, D. E. Cane, and C. Khosla, "An R-squared measure of goodness of fit for some common nonlinear regression models," *J. Econometrics*, vol. 77, no. 2, pp. 329–342, Apr. 1997.
[30] M. T. Orchard and C. A. Bouman, "Color quantization of images," *IEEE Trans. Signal Process.*, vol. 39, no. 12, pp. 2677–2690, Dec. 1991.
[31] G. Meng, Y. Wang, J. Duan, S. Xiang, and C. Pan, "Efficient image dehazing with boundary constraint and contextual regularization," in *Proc. IEEE Int. Conf. Comput. Vis.*, Dec. 2013, pp. 617–624.
[32] D. Berman, T. Treibitz, and S. Avidan, "Non-local image dehazing," in *Proc. IEEE Conf. Comput. Vis. Pattern Recognit. (CVPR)*, Jun. 2016, pp. 1674–1682.
[33] Y. Wang, W. Song, G. Fortino, L.-Z. Qi, W. Zhang, and A. Liotta, "An experimental-based review of image enhancement and image restoration methods for underwater imaging," *IEEE Access*, vol. 7, pp. 140233–140251, 2019.
[34] M. Yang and A. Sowmya, "An underwater color image quality evaluation metric," *IEEE Trans. Image Process.*, vol. 24, no. 12, pp. 6062–6071, Dec. 2015.
[35] K. Panetta, C. Gao, and S. Agaian, "Human-visual-system-inspired underwater image quality measures," *IEEE J. Ocean. Eng.*, vol. 41, no. 3, pp. 541–551, Jul. 2016.
[36] A. Mittal, A. K. Moorthy, and A. C. Bovik, "No-reference image quality assessment in the spatial domain," *IEEE Trans. Image Process.*, vol. 21, no. 12, pp. 4695–4708, Dec. 2012.
[37] S. Wang, K. Ma, H. Yeganeh, Z. Wang, and W. Lin, "A patch-structure representation method for quality assessment of contrast changed images," *IEEE Signal Process. Lett.*, vol. 22, no. 12, pp. 2387–2390, Dec. 2015.
[38] W. Ren, S. Liu, H. Zhang, J. Pan, X. Cao, and M. Yang, "Single image dehazing via multi-scale convolutional neural networks," in *Proc. Eur. Conf. Comput. Vis. (ECCV)*, Amsterdam, The Netherlands, 2016, pp. 154–169.
[39] D. Akkaynak, T. Treibitz, T. Shlesinger, Y. Loya, R. Tamir, and D. Iluz, "What is the space of attenuation coefficients in underwater computer vision?" in *Proc. IEEE Conf. Comput. Vis. Pattern Recognit. (CVPR)*, Jul. 2017, pp. 568–577.
[40] X. Zhao, T. Jin, and S. Qu, "Deriving inherent optical properties from background color and underwater image enhancement," *Ocean Eng.*, vol. 94, pp. 163–172, Jan. 2015.
[41] K. Tan and J. P. Oakley, "Physics-based approach to color image enhancement in poor visibility conditions," *J. Opt. Soc. Amer. A, Opt. Image Sci.*, vol. 18, no. 10, p. 2460, Oct. 2001.
[42] R. W. Austin and T. J. Petzold, "Spectral dependence of the diffuse attenuation coefficient of light in ocean waters," *Opt. Eng.*, vol. 25, no. 3, Mar. 1986, Art. no. 253471.
[43] W. Ren, J. Pan, H. Zhang, X. Cao, and M.-H. Yang, "Single image dehazing via multi-scale convolutional neural networks with holistic edges," *Int. J. Comput. Vis.*, vol. 128, no. 1, pp. 240–259, Jan. 2020.

YONGBIN LIU was born in Sanmenxia, Henan, China, in 1995. He received the B.S. degree in communication engineering from the Ocean University of China (OUC), Qingdao, China, in 2017, where he is currently pursuing the master's degree in communication and information systems. His research interests include image processing and underwater object recognition.

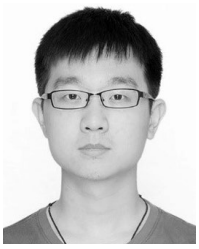

SHENGHUI RONG was born in Rizhao, Shandong, China, in 1989. He received the B.S. degree in electronic science and technology and the Ph.D. degree in physical electronics from Xidian University, Xi'an, China, in 2011 and 2018, respectively. In 2016, he was funded by the China Scholarship Council (CSC) to conduct Research in 3D image processing and recognition with Griffith University, Australia. He is currently a Lecturer with the School of Information Science and Engineering, Ocean University of China (OUC). His primary research interests include optoelectronic countermeasures, computer vision, and pattern recognition.

XUETING CAO was born in Ulanqab, Inner Mongolia, China, in 1996. She received the B.S. degree in electronic information science and technology from Inner Mongolia University, Inner Mongolia, China, in 2018. She is currently pursuing the master's degree in signal and information processing with the Ocean University of China, Qingdao, China. Her research interests include underwater image processing and underwater target recognition.

TENGYUE LI was born in Chaoyang, Liaoning, China, in 1990. He received the B.S. degree in electronic information science and technology and the M.S. degree in optical engineering from the Ocean University of China (OUC), Qingdao, China, in 2013 and 2015, respectively, where he is currently pursuing the Ph.D. degree in smart information and communication system. He has published two conference papers. He holds one Chinese invention patent and one Chinese utility model patent. His research interests include image processing, underwater 3D reconstruction, underwater object recognition, and underwater robotics technology.

BO HE (Member, IEEE) was born in Qingdao, Shandong, China, in 1971. He received the M.S. and Ph.D. degrees from the Harbin Institute of Technology, China, in 1996 and 1999, respectively. From 2000 to 2003, he was with Nanyang Technological University, Singapore, as a Postdoctoral Fellow. In 2004, he joined the Ocean University of China (OUC), where he is currently a Full Professor. He is also the Deputy Head with the Department of Electronic Engineering, School of Information Science and Engineering. His current research interests include precise navigation, control and communication for the platform of mobile robots, and unmanned vehicles, AUV design and applications, AUV SLAM, AUV control, and machine learning.